Front. Phys., 2012, 7(4): 408–417
DOI 10.1007/s11467-011-0225-9

REVIEW ARTICLE

Ferroelectricity generated by spin–orbit and spin–lattice couplings in multiferroic $DyMnO_3$

Na Zhang[1,2], **Shuai Dong**[3], **Jun-Ming Liu**[1,4,5,†]

[1] *Laboratory of Solid State Microstructures, Nanjing University, Nanjing 210093, China*
[2] *Department of Physics, Henan Normal University, Xinxiang 453007, China*
[3] *Department of Physics, Southeast University, Nanjing 211189, China*
[4] *Institute for Advanced Materials, South China Normal University, Guangzhou 510631, China*
[5] *International Center for Materials Physics, Chinese Academy of Sciences, Shenyang 110016, China*

E-mail: [†] *liujm@nju.edu.cn*

Received October 10, 2011; accepted November 4, 2011

While the ferroelectricity in type-II multiferroic rare-earth manganites is believed to be generated by the inverse Dzyaloshinskii–Moriya (DM) interaction (spin–orbit coupling) associated with the Mn spiral spin order, recent results revealed the strong spin–lattice coupling arising from the Dy–Mn spin interaction in $DyMnO_3$, which may also be an ingredient contributing to the ferroelectricity. In this work, we summarize our recent experiments on this issue by performing a series of rare-earth site nonmagnetic Y and magnetic Ho substitutions at Dy site for $DyMnO_3$. It is demonstrated that the Dy–Mn spin interaction contributes to the ferroelectric polarization through the symmetric exchange striction mechanism (spin–lattice coupling). A coexistence of the spin–orbit coupling and spin–lattice coupling in one compound is confirmed. At the same time, the independent Dy antiferromagnetic spin order at low temperature can be effectively suppressed by the substitutions, beneficial to the polarization enhancement.

Keywords multiferroics, spin–orbit coupling, spin–lattice coupling, coexistence

PACS numbers 75.85.+t, 75.30.Kz, 75.40.Cx, 75.47.Lx

Contents

1 Introduction 408
2 Magnetic structures of $DyMnO_3$ 410
3 Major motivations 411
4 Experimental details 411
5 Results and discussion 411
5.1 Structural stability 411
5.2 Multiferroicity of $DyMnO_3$ 411
5.3 Variations of magnetic property 412
5.4 Ferroelectricity upon the Y-substitution 413
5.5 Ferroelectricity upon the Ho-substitution 414
5.6 Discussion 415
6 Conclusions 415
Acknowledgements 415
References 416

1 Introduction

Multiferroics are a class of materials where electrical and magnetic properties coexist and are mutually coupled together, and they have been attracting a great deal of attention for decades, due to two major reasons: one is the fascinating physics underlying these coupled phenomena between the magnetic and ferroelectric orders, and the other is those promising potential applications in spintronics and data storages [1–7]. However, due to the exclusion issue between the ferroelectric order and magnetic one, such coexistence is usually rare and the magnetoelectric (ME) coupling, if any, is extremely weak, hindering the steps towards practical applications [8–10]. Tremendous efforts have been available in searching for alternatives so that the ME coupling is intrinsic and significant with high operation temperature, while substantial challenges remain even nowadays.

A crucial progress along this line is the discovery of the so-called type-II multiferroics (also coined as improper ferroelectrics) besides well known $BiFeO_3$. Among these multiferroics, orthorhombic ABO_3-type multiferroic manganites $R\mathrm{MnO}_3$ (R is trivalent rare-earth ion)

have attracted extensive interest, mainly due to the intrinsic ME coupling identified in these systems, in terms of the strongly coupled spin and ferroelectric orders as well as rich phase diagrams [10–25]. While it is believed that those well investigated multiferroics other than the type-II ones have their ferroelectricity and magnetism generated separately from different origins, here the ferroelectric (FE) polarization (P) in these type-II multiferroics is argued to originate from some second-order interactions between the spins and other orders of parameters (e.g., orbit, phonon), so that some specific spin orders may lead to breaking of the spatial inversion symmetry responsible for nonzero polarization. Therefore, the ME coupling in these multiferroics is intrinsic and also very significant, as repeatedly confirmed experimentally [10–21, 26].

So far, our understanding of the underlying microscopic mechanisms for the ferroelectricity generation in these type-II multiferroics remains preliminary, in particular no quantitative microscopic theory is yet available and phenomenological approach is in the early stage as well. As a highlight, two types of mechanisms are proposed which obtain support experimentally [3, 4, 16, 27]. One is the spin–orbit (SO) coupling associated with some specific spin orders such as spiral spin order, which leads to the antisymmetric exchange striction, taking $R\mathrm{MnO_3}$ where R =Tb, Dy, and $\mathrm{Eu}_{1-x}\mathrm{Y}_x$, as an example [10–16]. In details, due to the inverse Dzyaloshinskii–Moriya (DM) interaction associated with the Mn–O–Mn bond chains, the Mn spiral spin order allows a polarization $P_{\mathrm{so}} \sim \sum A\boldsymbol{e}_{ij} \times (S_i \times S_j) \sim \langle S_i \times S_j \rangle$, where $\boldsymbol{e}_{ij}$ denotes the unit vector connecting the two neighboring Mn spins (S_i and S_j) and the coefficient A is relevant to the spin–orbit coupling and complex superexchange interactions, and $\langle \cdots \rangle$ denotes the configuration averaging [16, 28–31]. We coin this term as the *cross-product term*. A schematic illustration of this SO coupling mechanism is given in Fig. 1(a), where only one piece of Mn–O–Mn chain is drawn. A nonzero P is clearly identified.

The other mechanism is relevant with the spin–phonon (SP) coupling, typically identified in $\mathrm{HoMnO_3}$, where the Mn spins favor the E-type antiferromagnetic (E-AFM) order [16, 32, 33]. The zigzag up-up-down-down ($\uparrow\uparrow\downarrow\downarrow$) spin alignment along the lattice diagonal direction on the Mn–O–Mn plane allows a nonzero P via the double-exchange induced symmetric exchangestriction [34, 35]. This component of P can be roughly expressed as $P_{\mathrm{sp}} \sim [S_i \cdot S_j]\boldsymbol{n}$, where S_i and S_j are the two neighboring spins and $\boldsymbol{n}$ is the polarization unit vector. This term is coined as the *dot-product term* here. The similar SP mechanism is also identified for Ising-like spin chain compound $\mathrm{Ca_3CoMnO_6}$ where the Co and Mn spins alternatively form the $\uparrow\uparrow\downarrow\downarrow$ spin chain along the c-axis, leading to a nonzero polarization along the c-axis [36–46]. Without losing generality, Fig. 1(b) illustrates one case where two types of charged ions align alternatively and the SP mechanism results in the collective ionic shifts, generating a polarization. Here it should be noted that the $\uparrow\uparrow\downarrow\downarrow$ spin alignment may not be a prerequisite for generating ferroelectricity and in principle a nonzero configuration averaging $[S_i \cdot S_j]\boldsymbol{n}$ over the whole lattice is sufficient for polarization generation.

It is interesting to find that these two microscopic mechanisms are identified separately in different individuals and the coexistence of them in one multiferroic system has been rarely revealed until recently. The exclusion of such coexistence in one system is based on different symmetries required respectively for the two types of mechanisms, while it cannot be possible to accommodate the two symmetries for the same spin order. Nevertheless, one possibility to overwhelm this exclusion is to accommodate two types of magnetic species in one system so as to allow the two mechanisms taking effect simultaneously. This sequence has obvious advantages. First, technologically the coexistence of both mechanisms allows opportunity to sum up the two components (P_{so} and P_{sp}) of polarization so that the total one is significantly enhanced with respect to the single one. Second, it is attractive to understand such coexistence, which represents a substantial step to uncover novel phenomena and physics associated with this coexistence. This is the major motivation for our recent experiments on

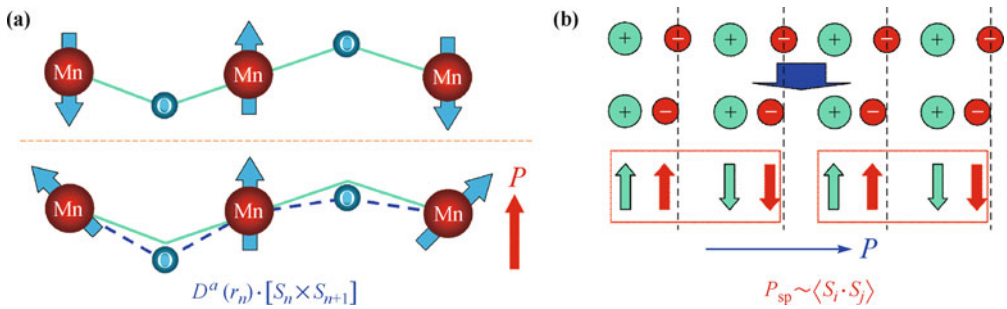

Fig. 1 **(a)** A schematic drawing of the Mn–O–Mn chain in manganites $R\mathrm{MnO_3}$. The upper panel shows the original AFM Mn–O–Mn chain without the DM interaction at temperature $T < T_{\mathrm{N}}$, the bottom panel displays the spin-noncollinear Mn–O–Mn chain due to the DM interaction, which induces the displacement of O ions perpendicular to the chain and thus FE polarization P at $T < T_{\mathrm{FE}}$. **(b)** A schematic drawing of the $\uparrow\uparrow\downarrow\downarrow$ spin chain constituted by two magnetic species in alternative alignment. The coherence ionic shifts due to the symmetric exchange striction and induced P are illustrated.

$DyMnO_3$ (DMO).

2 Magnetic structures of $DyMnO_3$

Keeping in mind the above motivation, one comes to highlight the already published data on the spin ordering sequence in DMO [10, 12, 18–25], and we outline the major facts about the magnetic structures of DMO under various conditions.

First of all, both the Dy ion and Mn ion are magnetic and in particular the Dy spin has a quite bigger moment ($\sim 10\mu_B$) than Mn spin [19, 22]. Upon decreasing temperature (T), the high-T paramagnetic state transits into an incommensurate (ICM) sinusoidal antiferromagnetic (AFM) state of the Mn spins at $T_N = 39$ K, below which the collinear Mn spin order is arranged first along the b-axis with propagation vector $\tau^{Mn} = (0, 0.36...0.385\boldsymbol{b}, 0)$ varying with temperature at $T < T_N$ [10, 19, 22]. What is interesting here is that slightly below T_N, the Dy-spins at the R-site also develop an AFM order along the c-axis with the same propagation vector as that of the Mn-spin order, i.e., $\tau^{Dy} = \tau^{Mn}$, duo to the strong coupling between the Dy-spin sublattice and the Mn-spin sublattice (Dy–Mn spin interaction) [18–21, 25]. This implies that the AFM Dy-spin ordering is induced by the Mn-spin order.

When T falls down further to $T_{FE} = 18$ K, an additional magnetic transition occurs, corresponding to the development of a spiral spin ordering (SSO) of the Mn-species along the b-axis [12, 19], with the fixed propagation vector $\tau^{Mn} = 0.385\boldsymbol{b}$ [21, 25]. The Dy-spins also develop a spiral spin order as a consequence of the strong coupling between the Dy-spin sublattice and the Mn-spin sublattice, under the premise of $\tau^{Dy} = \tau^{Mn} = 0.385\boldsymbol{b}$ [21]. The proposed magnetic structure projected on the bc-plane is schematically illustrated in Fig. 2(a). As addressed above, the spiral spin order of Mn ions allows a nonzero FE polarization, contributed from the *cross-product term* $P_{so} \sim \sum A\boldsymbol{e}_{ij} \times (S_i \times S_j)_{Mn}$ along the c-axis. Whether the spiral spin order of Dy ions makes a contribution to polarization P remains to be identified yet.

A surprising consequence of the magnetic structures is the coherence of spin configurations for Mn and Dy sublattices. Again consulting Fig. 2(a) for the proposed magnetic structures below T_{FE}, one finds that along the b-axis, the Mn spins between two neighboring Mn spin chains are anti-parallel, the same are the two neighboring Dy spin chains. If one considers the spin–lattice coupling between any Mn spin chain and its Dy spin chain neighbors, this coupling can be roughly expressed as a term $\sim (-1)^i(S^i_{Dy} \cdot S^i_{Mn})$, where i is an integer counting the Mn/Dy chain series along the c-axis. Therefore, the site-dependent configuration averaging over the whole lattice can be termed as $[S_{Dy} \cdot S_{Mn}]\boldsymbol{n}$, i.e., the *dot-product term*. A major issue arising from this discussion is whether this *dot-product term* associated with the spin–lattice coupling makes a contribution to ferroelectricity, i.e., a nonzero P_{sp} available?

An additional fact to be addressed for DMO is the independent Dy spin ordering below $T_{Dy} = 6.5$ K. In this case, the Dy spin order takes a commensurate AFM structure with propagation vector $\tau^{Dy} = 0.5\boldsymbol{b}$, irrelevant with the spiral spin order of Mn ions, as schematically illustrated in Fig. 2(b) [18, 22]. This independent Dy spin order implies the dominance of the Dy–Dy spin interaction over the Dy–Mn spin coupling at low $T < T_{Dy}$. The consequence of the competition between the two types of interactions may be the disappearance of component P_{sp} gradually at $T \to 0$ K. Surely, the Mn spiral spin structure (in particular the wave-vector) would be modulated by the Dy–Mn spin coupling in case of the independent Dy spin order, which is nevertheless different from that in case of the Dy spiral spin order at $T_{Dy} < T < T_{FE}$. One has a reason to expect that the polarization component (here denoted as P'_{so}) induced by the Mn spin–orbit coupling would be different from P_{so} at $T > T_{Dy}$.

Finally, we mention briefly the response of the magnetic structure to external magnetic field. Recent experiments revealed that at low $T < T_{Dy}$ external magnetic field first melts away the independent Dy spin order and

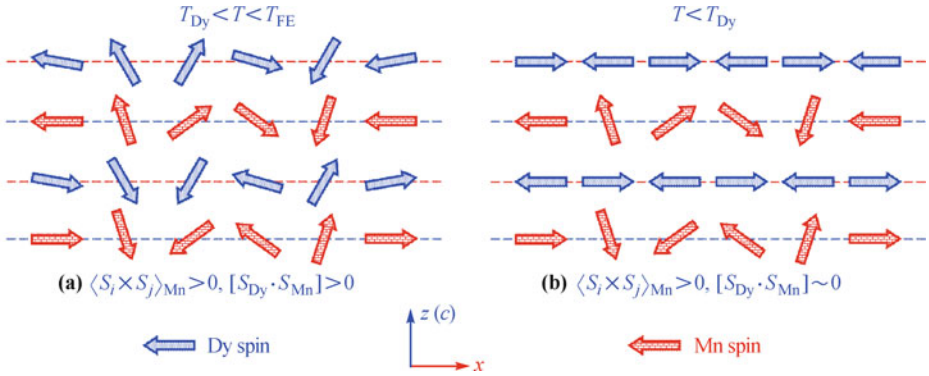

Fig. 2 A sketch of the ordered configurations of Dy-spins and Mn-spins, projected onto the zx-plane at temperatures **(a)** $T_{Dy} < T < T_{FE}$ and **(b)** $T < T_{Dy}$. The magnitude and orientation of these spin arrows are guides to the eyes.

then the Mn spiral spin order pluses the induced Dy spiral spin order, indicating the lower stability of the former than the latter. Keeping in mind above discussions, one would expect that an appropriate magnetic field which is sufficient to melt away the independent Dy spin order but insufficient to suppress the Mn/Dy spiral spin orders would help to recover the ferroelectric component $P_{\rm sp}$ at $T < T_{\rm Dy}$ [20].

3 Major motivations

To identify the above arguments, one may proceed with some simple approaches to separate the two components of the FE polarization by modulating the magnetic structures of DMO. The straight strategy is to substitute the Dy ion with various isovalent rare-earth species with and without magnetic moment.

On one hand, to isolate the *cross-product term* from the *dot-product term*, i.e., separate component $P_{\rm so}$ from $P_{\rm sp}$, one may substitute Dy with Y to some content. First, Y^{3+} has similar ionic size as Dy^{3+}, but Y^{3+} has much "weaker" magnetic moment than Dy^{3+} (if not zero). Such a substitution allows a suppression of both the Dy–Mn spin interaction and Dy–Dy spin interaction, and in turn the *dot-product term* and independent Dy spin ordering at $T < T_{\rm Dy}$. Given a sufficient substitution level which is however insufficient for changing the lattice symmetry, note that $YMnO_3$ favors the hexagonal symmetry, but the orthorhombic $YMnO_3$ structure can be maintained for specific conditions, and the component $P_{\rm sp}$ would become disappeared, leaving only the component $P_{\rm so}$. This is the first experiment to be described below.

On the other hand, it was reported that $HoMnO_3$ may also favor the orthorhombic symmetry under a well controlled condition [16, 47–49]. It was recently revealed that the ferroelectricity in orthorhombic $HoMnO_3$ may be generated due to the coupling between the Ho spins and Mn spins, probably via the spin–lattice coupling addressed above [34]. However, no independent Ho spin order appears at low T. Therefore, a proper low level substitution of Dy in $DyMnO_3$ with Ho may break gradually the independent Dy spin ordering at low T, while the *dot-product term* via the coupling between Mn spins and Dy/Ho spins can be maintained. In this case, both components $P_{\rm sp}$ and $P_{\rm so}$ are available over the whole T-range below $T_{\rm FE}$.

The present article reviews our experiments based on these motivations. Our experiments seem quite successful although the underlying physics may be even more complicated than the simple scenario given above.

4 Experimental details

Our experiments focus on polycrystalline $Dy_{1-x}Y_xMnO_3$ (DYMO) and $Dy_{1-y}Ho_yMnO_3$ (DHMO). These samples were synthesized by the conventional solid-state reaction route. The highest substitutions were determined to be $x = 0.2$ and $y = 0.3$, without causing identifiable impurity phase while maintaining the orthorhombic crystal structure. The phase purity and crystallinity were checked by X-ray diffraction (XRD) using Cu Kα radiation.

For detecting the spin ordering sequence, magnetization (M) and specific heat (C) of these samples were measured employing the Quantum Design superconducting quantum interference device (SQUID) and physical properties measurement system (PPMS), respectively. For ferroelectric characterizations, dielectric constant (ε) was measured using HP4294 impedance analyzer, and polarization P was evaluated from the measured T-dependence of pyroelectric current (I) using Keithley 6514 electrometer in combination with PPMS. As a poling procedure, each sample was first cooled down to 2 K under an electric field (E) of 10 kV/cm, followed by a sufficiently long time of circuit-shorting for safe exclusion of other possible contributions such as those from the de-trapped charges. Finally, the measured pyroelectric current was integrated as a function of time to obtain polarization P. In addition, the response of P against magnetic field H was also probed using the same method.

5 Results and discussion

While it should be mentioned that the main part of the data have already been published [50, 51], we present them in an integrated scenario for both the Y substitution and Ho one.

5.1 Structural stability

We look at the orthorhombic structural stability of DMO upon the Y- and Ho-substitutions. The probed XRD spectra for the DYMO and DHMO samples at room temperature are shown in Figs. 3(a) and (b), with the values of x and y inserted in the plots respectively. A careful check of these data in assistance with the Rietveld structure refining reveals that the orthorhombic symmetry can be maintained up to $x = 0.20$ and $y = 0.30$. A slight shift of these reflections towards the high-angle side is identified, as shown in the insets, with a notice that the ionic radius values of Y^{3+} and Ho^{3+} are ~ 0.9 Å and ~ 0.901 Å, respectively, smaller than 0.912 Å, the radius of Dy^{3+}.

5.2 Multiferroicity of $DyMnO_3$

For a comprehensive understanding of the effects of Y- and Ho-substitutions on DMO, we first summarize our

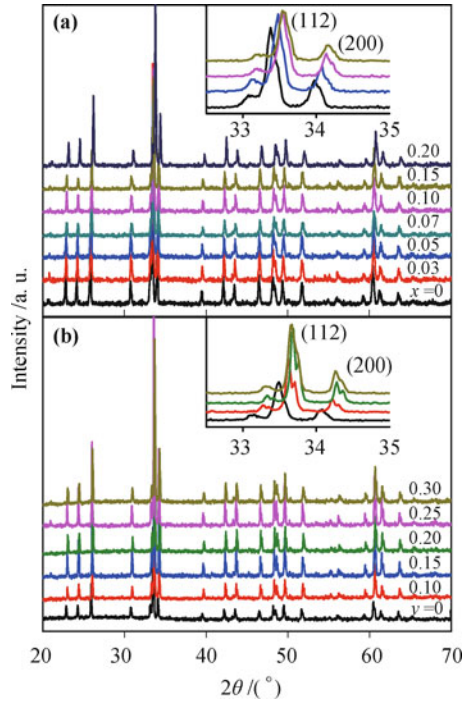

Fig. 3 X-ray diffraction patterns for pure and substituted samples, with the substation levels labeled numerically. The inset clarifies the (112) and (200) peaks for **(a)** $x = 0, 0.05, 0.10, 0.15$ and **(b)** $y = 0, 0.1, 0.2, 0.3$ from bottom to up, respectively.

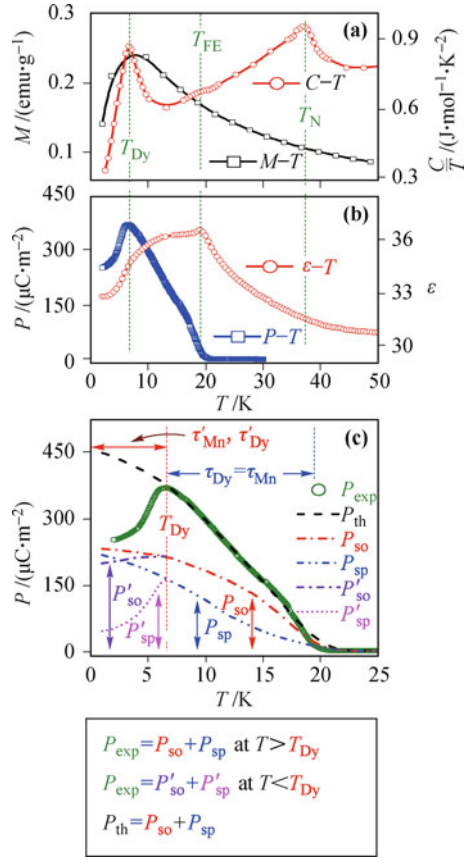

Fig. 4 Measured **(a)** M and C/T, **(b)** ε and P, as a function of T, respectively, for pure DMO. **(c)** A sketch map of the T-dependences of various polarization components of DMO. P_{so} and P'_{so} represent the contributions from the spiral order of Mn spins with different wave vectors, P'_{sp} and P_{sp} the contributions from the spin–lattice coupling arising from the Dy–Mn spin coupling with and without the impact from the independent Dy ordering, and P_{exp} and P_{th} the total polarizations from measurement and theoretical estimation (assuming no independent Dy ordering in low T).

data on the multiferroicity of DMO in Fig. 4, as a reference.

The measured M–T data and C/T–T data for DMO are plotted in Fig. 4(a), respectively, which show quite good consistence with earlier reports on DMO [10, 12, 18–25]. The $M(T)$ curve shows no identifiable anomaly around T_N and T_{FE}, leaving only a broad peak at $T \sim T_{Dy} \sim 7$ K associated with the independent Dy spin order. This phenomenon is reasonable since the magnetic moment of Dy^{3+} is much bigger than Mn^{3+}, and thus no identifiable magnetic signal from the Mn spin ordering is possible from the magnetization data. We thus turn to the specific heat C for consult, which is more sensitive to spin ordering. Indeed, sharp peaks at $T \sim T_N$ and T_{Dy} and a relatively weak anomaly at $T \sim T_{FE}$ are detected, corresponding to the three spin ordering events.

More attentions go to the measured P–T and ε–T curves at zero magnetic field, as shown in Fig. 4(b). The dielectric peak at $T \sim T_{FE}$ indicates the ferroelectric transitions at which a nonzero P ensues. The measured P rises continuously with decreasing T until T_{Dy}, beyond which it decays rapidly down to a finite value. The one-to-one correspondence between the features in the P–T, ε–T, and C/T–T curves clearly demonstrates the intrinsic ME effect in DMO.

Based on the scenario on the two polarization components (P_{so} and P_{sp}) arising respectively from the *cross-product term* and *dot-product term*, one may suggest in a qualitative sense the dependence of P_{so} and P_{sp} on T, as shown in Fig. 4(c). Below T_{FE} down to zero, the measured value of P, P_{exp}, and the predicted value of P, P_{th}, can be expressed as:

$$P_{exp} = \begin{cases} P_{so} + P_{sp}, & T_{Dy} < T < T_{FE} \\ P'_{so} + P'_{sp}, & T < T_{Dy} \end{cases} \qquad (1)$$
$$P_{th} = P_{so} + P_{sp}, \quad T < T_{FE}$$

It is seen that both P_{so} and P_{sp} would increase monotonously with decreasing T if no independent Dy spin ordering occurs below T_{Dy}. Nevertheless, due to this Dy spin ordering, P_{sp} transits into P'_{sp} below T_{Dy}, which gradually decays down to zero since the synchronization of the Dy spin order with the Mn spin order phases out below T_{Dy}, such that the *dot-product term* approaches zero. Eventually, at $T \to 0$ K, only the component P'_{so} arising from the Mn spin order is left. In the following subsections, we shall present our experimental data to support this scenario.

5.3 Variations of magnetic property

As mentioned above, both Dy^{3+} and Ho^{3+} spins have

much bigger moment than Mn^{3+} spin [19, 20, 52], thus no information on the response of the Mn spin ordering to the substitutions can be obtained in case of relatively low level Y/Ho substitution levels. Nevertheless, one can still observe the variation of the measured M upon the substitutions, as shown in Fig. 5 where the M–T data for several Y/Ho-doped samples are plotted. First of all, no substantial difference between the data under the ZFC and FC modes for all the samples can be detected, indicating the robustness of the spin order upon the substitutions. Second, both the Y- and Ho-substitutions suppress the independent Dy spin ordering which can be initiated only at lower T, with the peaks at T_{Dy} indicated by the arrows.

Furthermore, looking at the response of M to the substitutions, as shown in Figs. 5(b) and (c), one observes the down-shift and up-shift of the M–T curves respectively with increasing x and y, while both cases show downshifting T_{Dy}. A reasonable explanation is that Y^{3+} spin has much smaller moment but Ho^{3+} spin has slightly bigger one than the Dy^{3+} spin.

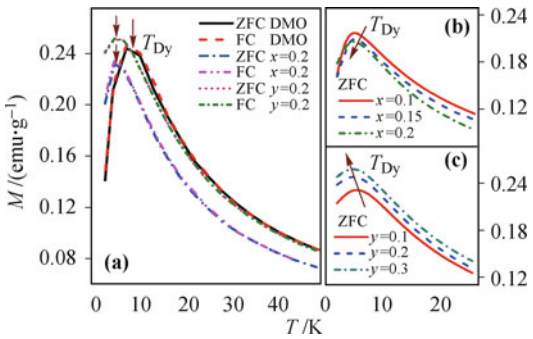

Fig. 5 Measured M–T curves **(a)** for samples $x = 0$, $x = 0.2$, and $y = 0.2$ under ZFC and FC conditions, **(b)** for samples with $0.1 \leqslant x \leqslant 0.2$ and **(c)** for samples with $0.1 \leqslant y \leqslant 0.3$ under ZFC conditions. $H = 100$ Oe.

5.4 Ferroelectricity upon the Y-substitution

In this section we address in details the response of polarization P to the Y-substitution (x). The measured data are summarized in Fig. 6 which shows the C/T–T curves of three samples, illustrating the impact of the substitution on the three transition points, T_N, T_{FE}, and T_{Dy}. It is again confirmed that the substitution suppresses the independent Dy spin ordering while T_N increases due to the higher AFM ordering point of orthorhombic $YMnO_3$ than $DyMnO_3$ [16, 34]. A slight decrease of T_{FE} is also observed.

Regarding the variation of P as a function of T in response to the substitution, at the beginning the measured P falls down over the whole T-range until $x \sim 0.10$, beyond which no more change of P within $T_{Dy} < T < T_{FE}$, while the P below T_{Dy} gradually rebounds back to a higher value, as shown in Figs. 6(b) and (c). The different behaviors of $P(T)$ at the two sides of T_{Dy} reflect the influence of the independent Dy spin order on the ferroelectricity. To illustrate this fact, we plot P as a function of x at $T = 2$ K and 10 K, below and above T_{Dy}, respectively, in Fig. 6(d).

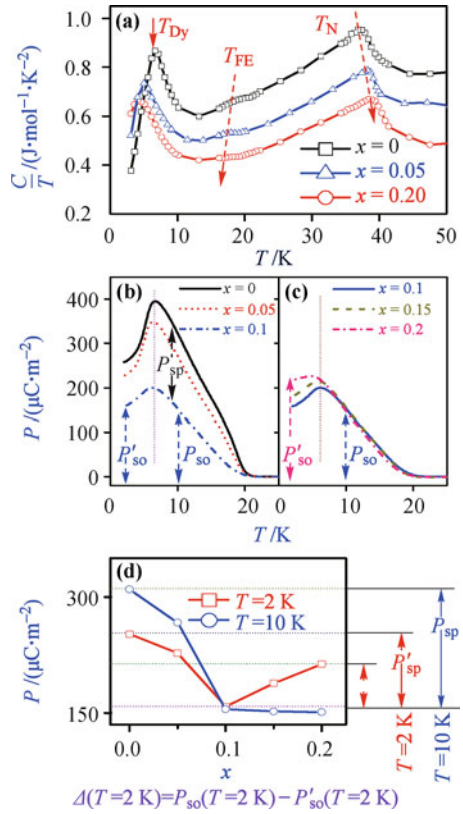

Fig. 6 **(a)** Measured $C/T-T$ curves for samples with $x = 0, 0.05$, and 0.2. **(b)** and **(c)** Measured P–T curves for samples with $x = 0, 0.05, 0.1, 0.15$, and 0.2. **(d)** Measured P–x curves at fixed $T = 2$ K and 10 K.

We consult the proposed scenario shown in Fig. 4(c) and Eq. (1) in order to explain the effects of the Y-substitution. The substitution gradually melts the Dy spin order below T_{FE} no matter whether it is induced by Mn spin order ($T_{Dy} < T < T_{FE}$) or develops independently (below T_{Dy}). This leads to the gradual collapse of the Dy–Mn spin coupling, i.e., the *dot-product term* is gradually suppressed. In the meantime, the low-T independent Dy spin order seems to be more robust than the Dy spin order at $T_{Dy} < T < T_{FE}$, which is induced by the Mn spin order. Therefore, the substitution level needed to completely melt away the independent Dy spin order at $T < T_{Dy}$ is higher than that required to break the Mn spin order induced Dy spin order at $T_{Dy} < T < T_{FE}$. This suggests that a transition from P'_{so} to P_{so} at $T < T_{Dy}$ cannot occur unless $x > 0.10$, i.e., further increase of x from 0.10 results in the rebound of P.

As a supplementary, the spin configurations associated with the Y-substitution are schematically shown in Fig. 7. Referring to Fig. 2, the physics of the substitution is quite clear and the Y-substitution breaks the Dy SSO configuration at $T_{Dy} < T < T_{FE}$ and the independent Dy spin order at $T < T_{Dy}$, respectively. Based on our data

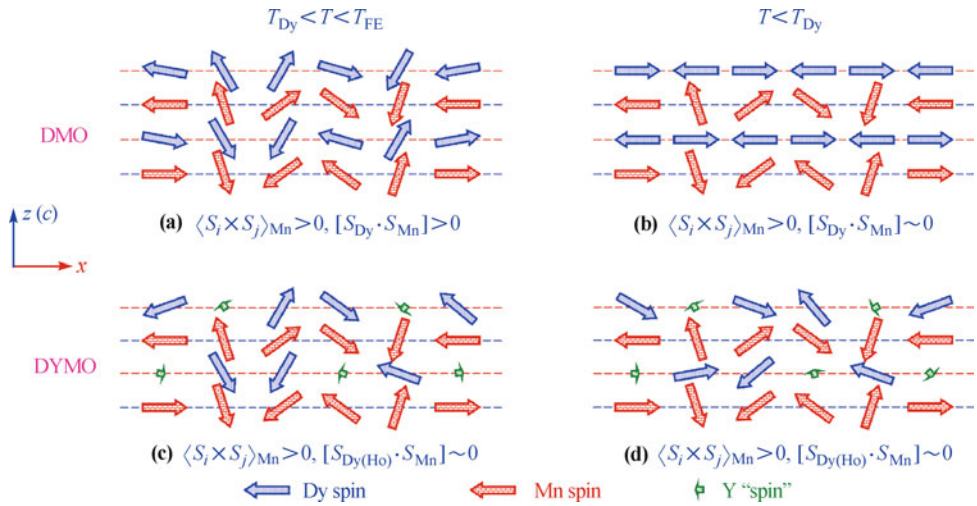

Fig. 7 A sketch of the ordered configurations of Dy-spins and Mn-spins for DMO and DYMO, projected onto the zx-plane at temperatures **(a)** $T_{Dy} < T < T_{FE}$ and **(b)** $T < T_{Dy}$. The magnitude and orientation of these spin arrows are guides to the eyes.

and Fig. 7, the multiferroic phase diagram in the (T, x) plane for DYMO system can be drawn and is shown in Fig. 8.

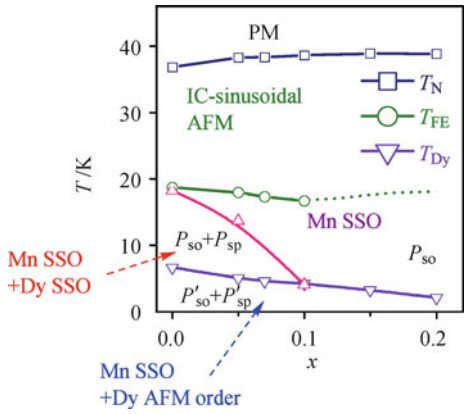

Fig. 8 The T–x phase diagram of DYMO with Y substitution $0 \leqslant x \leqslant 0.2$ [50].

5.5 Ferroelectricity upon the Ho-substitution

Based on the above results, one can expect obviously that the Ho-substitution would suppress gradually the independent Dy spin order at $T < T_{Dy}$, but the *dot-product term* may be maintained. Therefore, if the independent Dy spin order is completely suppressed by the Ho-substitution, Eq. (1) can be rewritten as

$$P_{exp} = P_{th} = P_{so} + P_{sp}, \quad T < T_{FE} \tag{2}$$

Our experimental results are summarized in Fig. 9 where the C/T–T and P–T data for four samples are plotted in (a) and (b). From the C/T–T data, it is seen that the independent Dy spin order is already melt away at $y \sim 0.1$ and over. The AFM ordering point T_N shifts slightly towards the high-T side, while the T_{FE} towards the low-T side slightly with the increasing y, with a notice that the orthorhombic $HoMnO_3$ has a higher T_N than that of DMO. The anomaly of C/T at $T \sim T_{FE}$ clearly evidences the Mn spiral spin ordering which is not affected by the Ho-substitution.

More convincingly, the measured P at $T < T_{Dy}$ does rebound back with increasing y and eventually $P'_{sp} \to P_{sp}$ and $P'_{sp} \to P_{so}$ at $y > 0.1$. The P–T curve no longer falls down at low T and tends to a saturated value: a sum of the component P_{so} and component P_{sp}. In Fig. 9(c) is shown the measured P as a function of y at $T = 2$ K and the Ho-substitution does induce significant enhancement

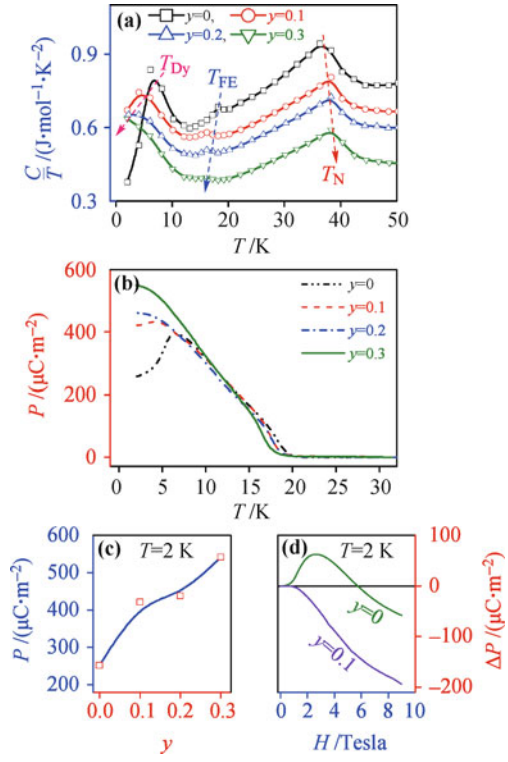

Fig. 9 **(a)** Measured C/T–T curves for samples with $y = 0, 0.1, 0.2$, and 0.3. **(b)** Measured P–T curves for samples with $y = 0, 0.1, 0.2$, and 0.3. **(c)** Measured P–y curve at $T \sim 2$ K. **(d)** Measured dependence of ΔP on H at $T \sim 2$ K for samples $y = 0$ and $y = 0.1$.

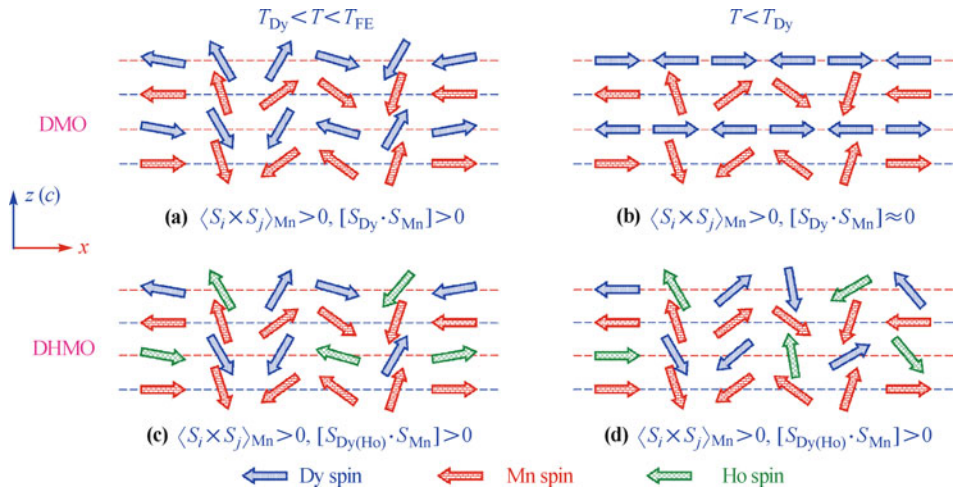

Fig. 10 A sketch of the ordered configurations of Dy-spins and Mn-spins for DMO and DHMO, projected onto the zx-plane at temperatures **(a)** $T_{Dy} < T < T_{FE}$ and **(b)** $T < T_{Dy}$. The magnitude and orientation of these spin arrows are guides to the eyes [51].

of P at low T.

In addition, the response of P at $T = 2$ K [$\Delta P = P(H) - P(0)$] to external magnetic field H for two samples ($y = 0$ and 0.1) is plotted in Fig. 9(d). For the sample $y = 0$ (DMO), a magnetic field first suppresses the independent Dy spin order, which allows the re-entrance of the Dy spin order induced by the Mn spiral spin order. This is the reason why ΔP is positive first and then negative with increasing H. This phenomenon disappears for the sample $y = 0.1$, where the independent Dy spin order is no longer dominant, thus ΔP falls down monotonously with increasing H.

What should be mentioned is that the Ho-substitution does not damage the *dot-product term*. Instead, the Ho^{3+} ions substitute the Dy^{3+} ions and it seems that the Dy–Mn spin coupling is substituted by the Ho–Mn spin coupling [24], which would also contribute to the *dot-product term*. Such a coupling in fact was recently confirmed by experiments on $HoMnO_3$ [34, 53].

To illustrate this effect, we present the spin configuration of DHMO in Figs. 10(c) and (d), with that of DMO shown in Figs. 10(a) and (b). It is seen that at $T_{Dy} < T < T_{FE}$ the *dot-product term* is reserved via the Dy–Mn and Ho–Mn spin coupling, but the independent Dy spin order at $T < T_{Dy}$ is broken.

5.6 Discussion

Up to this stage, we have developed a comprehensive scenario in which the mechanism for ferroelectricity in $DyMnO_3$ can be well understood. The coexisting Mn–Mn spin interaction and Dy–Mn spin interaction allow a superposition of the polarization components as generated respectively from the *cross-product term* and *dot-product term*. The present work seems to be the first demonstration of this superposition. Furthermore and probably more importantly, the superposition is favored only if the two polarization components align along the same orientation, which would be cancelled otherwise. Fortunately it is the case for $DyMnO_3$. The similar scenario for other multiferroic manganites with two magnetic species is believed, i.e., the spin coupling between the two species may serve as a general mechanism for ferroelectricity generation. Surely, additional exploration is definitely needed.

On the other hand, the specific spin configuration for the *cross-product term* and *dot-product term* is only one of the necessary conditions for the ferroelectricity. The lattice symmetry and distortion should be another substantial ingredient for nonzero polarization. In the present case, both $YMnO_3$ and $HoMnO_3$ can be of orthorhombic structure in spite of the meta-stability, and both Y^{3+} and Ho^{3+} have similar ionic size as Dy^{3+}, which would not add additional degree of freedom for the structure control.

6 Conclusions

In summary, we have thoroughly investigated the multiferroic properties of $DyMnO_3$ substituted with isovalent Y^{3+} and Ho^{3+}. We have succeeded in revealing the entire microscopic mechanisms for the ferroelectricity generation in $DyMnO_3$, and have clearly revealed the cooperative contributions of spin–orbit (SO) coupling and spin–lattice (SP) coupling to the ferroelectricity. The feasibility of coexistence of the SO and SP couplings in one cyclodial order is the spin coupling between two magnetic species, which is generic and allows us opportunity to design and modulate the multiferroic properties of the type-II multiferroics.

Acknowledgements This work was supported by the National Natural Science Foundation of China (Grant Nos. 50832002, 11004027, and 11074113) and the National Key Projects for

Basic Research of China (Grant Nos. 2011CB922101 and 2009CB929501).

References

1. M. Fiebig, J. Phys. D, 2005, 38(8): R123
2. W. Eerenstein, N. D. Mathur, and J. F. Scott, Nature, 2006, 442(7104): 759
3. S. W. Cheong and M. Mostovoy, Nat. Mater., 2007, 6(1): 13
4. K. F. Wang, J. M. Liu, and Z. F. Ren, Adv. Phys., 2009, 58(4): 321
5. M. Bibes and A. Barthélémy, Nat. Mater., 2008, 7(6): 425
6. M. Gajek, M. Bibes, S. Fusil, K. Bouzehouane, J. Fontcuberta, A. Barthélémy, and A. Fert, Nat. Mater., 2007, 6(4): 296
7. W. Prellier, M. P. Sing, and P. Murugavel, J. Phys.: Condens. Matter, 2005, 17(30): R803
8. N. A. Hill, J. Phys. Chem. B, 2000, 104(29): 6694
9. H. Schmid, Magnetoelectric Effects in Insulationg Magnetic Materials, in: Introduction to Complex Mediums for Optics and Electromagnetics, edited by W. S. Weiglhoger and A. Lakhtakia, Bellingham, WA: SPIE Press, 2003: 167
10. T. Kimura, G. Lawes, T. Goto, Y. Tokura, and A. P. Ramirez, Phys. Rev. B, 2005, 71(22): 224425
11. T. Kimura, T. Goto, H. Shintani, K. Ishizaka, T. Arima, and Y. Tokura, Nature, 2003, 426(6962): 55
12. T. Goto, T. Kimura, G. Lawes, A. P. Ramirez, and Y. Tokura, Phys. Rev. Lett., 2004, 92(25): 257201
13. M. Kenzelmann, A. B. Harris, S. Jonas, C. Broholm, J. Schefer, S. B. Kim, C. L. Zhang, S. W. Cheong, O. P. Vajk, and J. W. Lynn, Phys. Rev. Lett., 2005, 95(8): 087206
14. J. Hemberger, F. Schrettle, A. Pimenov, P. Lunkenheimer, V. Yu. Ivanov, A. A. Mukhin, A. M. Balbashov, and A. Loidl, Phys. Rev. B, 2007, 75(3): 035118
15. J. A. Moreira, A. Almeida, W. S. Ferreira, J. P. Araújo, A. M. Pereira, M. R. Chaves, M. M. R. Costa, V. A. Khomchenko, J. Kreisel, D. Chernyshov, S. M. F. Vilela, and P. B. Tavares, Phys. Rev. B, 2010, 82(9): 094418
16. S. Ishiwata, Y. Kaneko, Y. Tokunaga, Y. Taguchi, T. Arima, and Y. Tokura, Phys. Rev. B, 2010, 81(10): 100411(R)
17. J. Strempfer, B. Bohnenbuck, M. Mostovoy, N. Aliouane, D. N. Argyriou, F. Schrettle, J. Hemberger, A. Krimmel, and M. V. Zimmermann, Phys. Rev. B, 2007, 75(21): 212402
18. N. Aliouane, O. Prokhnenko, R. Feyerherm, M. Mostovoy, J. Strempfer, K. Habicht, K. Rule, E. Dudzik, A. U. B. Wolter, A. Maljuk, and D. N. Argyriou, J. Phys.: Condens. Matter, 2008, 20(43): 434215
19. O. Prokhnenko, R. Feyerherm, E. Dudzik, S. Landsgesell, N. Aliouane, L. C. Chapon, and D. N. Argyriou, Phys. Rev. Lett., 2007, 98(5): 057206
20. R. Feyerherm, E. Dudzik, A. U. B. Wolter, S. Valencia, O. Prokhnenko, A. Maljuk, S. Landsgesell, N. Aliouane, L. Bouchenoire, S. Brown, and D. N. Argyriou, Phys. Rev. B, 2009, 79(13): 134426
21. E. Schierle, V. Soltwisch, D. Schmitz, R. Feyerherm, A. Maljuk, F. Yokaichiya, D. N. Argyriou, and E. Weschke, Phys. Rev. Lett., 2010, 105(16): 167207
22. R. Feyerherm, E. Dudzik, N. Aliouane, and D. N. Argyriou, Phys. Rev. B, 2006, 73(18): 180401(R)
23. N. Zhang, K. F. Wang, S. J. Luo, T. Wei, X. W. Dong, S. Z. Li, J. G. Wan, and J. M. Liu, Appl. Phys. Lett., 2010, 96(25): 252902
24. O. Prokhnenko, N. Aliouane, R. Feyerherm, E. Dudzik, A. U. B. Wolter, A. Maljuk, K. Kiefer, and D. N. Argyriou, Phys. Rev. B, 2010, 81(2): 024419
25. R. Feyerherm, E. Dudzik, O. Prokhnenko, and D. N. Argyriou, J. Phys.: Conf. Ser., 2010, 200(1): 012032
26. Y. Yamasaki, H. Sagayama, T. Goto, M. Matsuura, K. Hirota, T. Arima, and Y. Tokura, Phys. Rev. Lett., 2007, 98(14): 147204
27. T. Kimura, S. Ishihara, H. Shintani, T. Arima, K. T. Takahashi, K. Ishizaka, and Y. Tokura, Phys. Rev. B, 2003, 68(6): 060403 (R)
28. H. Katsura, N. Nagaosa, and A. V. Balatsky, Phys. Rev. Lett., 2005, 95(5): 057205
29. M. Mostovoy, Phys. Rev. Lett., 2006, 96(6): 067601
30. I. A. Sergienko and E. Dagotto, Phys. Rev. B, 2006, 73(9): 094434
31. S. Dong, R. Yu, S. Yunoki, J. M. Liu, and E. Dagotto, Phys. Rev. B, 2008, 78(15): 155121
32. I. A. Sergienko, C. Sen, and E. Dagotto, Phys. Rev. Lett., 2006, 97(22): 227204
33. S. Picozzi, K. Yamauchi, B. Sanyal, I. A. Sergienko, and E. Dagotto, Phys. Rev. Lett., 2007, 99(22): 227201
34. B. Lorenz, Y. Q. Wang, and C. W. Chu, Phys. Rev. B, 2007, 76(10): 104405
35. C. Y. Ren, Phys. Rev. B, 2009, 79(12): 125113
36. Y. J. Choi, H. T. Yi, S. Lee, Q. Huang, V. Kiryukhin, and S. W. Cheong, Phys. Rev. Lett., 2008, 100(4): 047601
37. V. Kiryukhin, S. S. Lee, Q. Ratcliff, H. T. Huang, Y. J. Yi, Y. Choi, and S. W. Cheong, Phys. Rev. Lett., 2009, 102(18): 187202
38. Y. J. Jo, S. S. Lee, E. S. Choi, H. T. Yi, Y. J. Ratcliff, V. Choi, S. W. Kiryukhin, S. Cheong, and L. Balicas, Phys. Rev. B, 2009, 79(1): 012407
39. R. Flint, H. T. Yi, P. Chandra, S. W. Cheong, and V. Kiryukhin, Phys. Rev. B, 2010, 81(9): 092402
40. Y. J. Guo, S. Dong, K. F. Wang, and J. M. Liu, Phys. Rev. B, 2009, 79(24): 245107
41. H. Wu, T. Burnus, Z. Hu, C. Martin, A. Maignan, J. C. Cezar, A. Tanaka, N. B. Brookes, D. I. Khomskii, and L. H. Tjeng, Phys. Rev. Lett., 2009, 102(2): 026404
42. X. Y. Yao, V. C. Lo, and J. M. Liu, J. Appl. Phys., 2009, 105(3): 033907
43. X. Y. Yao, V. C. Lo, and J. M. Liu, J. Appl. Phys., 2009, 106(1): 013903
44. Y. Zhang, H. J. Xiang, and M. H. Whangbo, Phys. Rev. B, 2009, 79(5): 054432

45. L. Li, W. Z. Luo, Y. J. Guo, S. Z. Li, S. J. Luo, K. F. Wang, and J. M. Liu, Appl. Phys. Lett., 2010, 96(2): 022516
46. P. Ding, L. Li, Y. J. Guo, Q. Y. He, X. S. Gao, and J. M. Liu, Appl. Phys. Lett., 2010, 97(3): 032901
47. B. Lorenz, Y. Q. Wang, Y. Y. Sun, and C. W. Chu, Phys. Rev. B, 2004, 70(21): 212412
48. J. S. Zhou, J. B. Goodenough, J. M. Gallardo-Amores, E. Morán, M. A. Alario-Franco, and R. Caudillo, Phys. Rev. B, 2006, 74(1): 014422
49. H. W. Brinks, H. Fjellvåg, and A. Kjekshus, J. Solid State Chem., 1997, 129(2): 334
50. N. Zhang, S. Dong, G. Q. Zhang, L. Lin, Y. Y. Guo, J. M. Liu, and Z. F. Ren, Appl. Phys. Lett., 2011, 98(1): 012510
51. N. Zhang, Y. Y. Guo, L. Lin, S. Dong, Z. B. Yan, X. G. Li, and J. M. Liu, Appl. Phys. Lett., 2011, 99(10): 102509
52. A. Munoz, M. T. Casais, J. A. Alonso, M. J. Martinez-Lope, J. L. Martinez, and M. T. Fernandez-Diaz, Inorg. Chem., 2001, 40(5): 1020
53. G. Q. Zhang, S. J. Luo, S. Dong, Y. J. Gao, and J. M. Liu, J. Appl. Phys., 2011, 109: 07D901